Int. J. Electrochem. Sci., 12 **(2017)** 11515 – 11527, doi: 10.20964/2017.12.21

International Journal of
ELECTROCHEMICAL
SCIENCE
www.electrochemsci.org

Electrochemical and Passivation Behavior of Duplex Stainless Steel in Simulated Concrete Pore Solution

Jian WANG[*], *Xinyu LIU, Zonglin YI, Peide HAN*[*]

College of Materials Science and Engineering, Taiyuan University of Technology, Tai yuan 030024, Shanxi, China;
[*]E-mail: jianwang1@126.com, hanpeide@126.com

Received: 18 July 2017 / *Accepted:* 4 October 2017 / *Published:* 12 November 2017

Corrosion of steel bars is an important cause of damage to concrete structures, and the passivation films formed on the surface of steel bars could play an effectively protective effect against corrosion. In this study, the common passivation intervals of the 2101, the 2205 and the 2304 duplex stainless steels were determined through cyclic voltammetry and potentiodynamic polarization in simulated concrete pore solution. Following the electrochemical impedance spectroscopy, the results demonstrated that three types of duplex stainless steels formed the most stable passivation film at the -0.2V polarization potential. Finally, the passive film formed on the surface of the three duplex stainless steels, was characterized through the Mott-Schottky and XPS analysis. The experimental data demonstrated that the corrosion resistance of the 2205 duplex stainless steel was improved compared to the 2101 and 2304 duplex stainless steels at the -0.2V polarization potential in the simulated concrete pore solution. This was relative to the alloy composition that generated the formed passive film difference.

Keywords: concrete structure; duplex stainless steel; passive film; electrochemical tests.

1. INTRODUCTION

The steel corrosion is one of the most important issues that may cause the service life degradation of concrete structures [1]. In order to solve this issue, the concrete structure was often reinforced by the stainless steel addition into the corresponding key parts, due to the excellent corrosion resistance and mechanical properties [2, 3]. The pore solution of concrete often consists of a alkaline mixture phase that is essentially a $Ca(OH)_2$ saturated solution along with amounts of KOH and NaOH, which leads to the formation of protective passive film on the surface of reinforcing steel. Despite all this, chloride attack and carbonation are inevitable in the concrete reinforcement through steel embedding, penetrating the passive film and eventually causing the corrosion failure of steel [4-6].

Due to the higher mechanical and corrosion resistance compared to the traditional stainless steel, the duplex stainless steel (DSS) has been widely applied in many fields, including oil, petrochemical, desalinator and paper mills [7, 8]. A high number of studies have been implemented to explore the effect of the corresponding composition, morphology, microstructure and precipitated phases on the mechanical and corrosion properties. Currently, certain researches have focused on the electrolyte solutions effect on the corrosion resistance of duplex stainless steels in concrete structures. In few works, the corrosion resistance performances of DSS in alkaline solutions with different pH or chloride contents were compared [9, 10]. Certain studies indicated the pitting nucleation position existence of DSS in simulated concrete pore solutions [11]. In several researches, the role of alloying elements on the pitting corrosion of the DSS reinforced cement structure was also discussed [12].

It is well known that the excellent corrosion resistance of DSS benefit from the passive film as a barrier layer against aggressive corrosion from the environment. The nature and stability of passive films often contain the film thickness, the stoichiometry, the microstructure and the electronic properties [13, 14]. In order to understand the passive film characterization, the most typical method is the electrochemical study [15-17]. Besides this method, certain other characterizations, such as x-ray photoelectron spectroscopy (XPS)[18], Raman spectroscopy[19] and Auger electron spectroscopy (AES)[20], were also presented in the reported literatures to analyze the passive films. These researches have demonstrated t that the passive films of the DSS were highly affected by many factors, including residual stresses, grain size, temperature and precipitated phase [21-26]. A protective oxide layer would be spontaneously formed on the steel surface in concrete, whereas the structure and passive properties of steels were proved to be affected by the different electrolyte systems. However, a low number of studies on the passive behavior of duplex steels in concrete constructions exist.

The purpose of this paper was to obtain a full understanding of the passive behavior of the 2101, 2304 and 2205 duplex stainless steels in a simulated concrete pore solution. The cyclic voltammetry and potentiodynamic polarization curves were firstly utilized to determine the passive ranges of duplex steels in the simulated concrete pore solution. The electrochemical impedance spectroscopy was implemented to obtain the steady state conditions for the formation of passive films at different anodic potentials. The Mott-Schottky curves and XPS analysis were finally employed to explain the different corrosion resistances of the passive films formed on the 2101, 2205 and 2304 samples.

2. EXPERIMENTAL

2.1 Specimen preparation

Table 1. Chemical composition of the 2101, 2205 and 2304 (wt. %)

Materials	Composition in Wt.%									
	C	Si	Mn	P	S	Cr	Ni	Mo	N	Fe
2101	0.02	0.50	5.46	0.03	0.0017	21.76	1.50	0.16	0.14	Bal.
2205	0.02	0.65	1.37	0.014	0.0008	22.36	5.21	3.18	0.15	Bal.
2304	0.02	0.35	1.49	0.025	0.0010	23.23	4.8	0.42	0.12	Bal.

The DSS utilized used in this study were typical 2101, 2205 and 2304 steels that were supplied by the Taiyuan iron&steel company Ltd. (TISCO). The chemical compositions of the DSS are presented in Table 1. All specimens were cut into low-sized blocks with a size of 1 cm ×1 cm and solution-treated at 1323 K for 1 h, also quickly quenched in water. Subsequently, each sample was mounted in epoxy resin; mechanically ground with SiC papers from 120 to 3000 grit, polished to mirror finish, and subsequently cleaned through distilled water and ethanol.

2.2 Electrochemical measurements

The electrochemical experiments were performed in a simulated concrete pore solution which was composed of 0.1 mol/L NaOH + 0.2 mol/L KOH + 0.1 mol/L $Ca(OH)_2$ + 0.003 mol/L $CaSO_4$ with a PH of approximately 13.3 at room temperature and atmospheric pressure. This was achieved with a three-electrode corrosion cell equipped with a saturated calomel electrode (SCE) reference electrode and a platinum foil counter electrode. The deionized water was utilized as the solvent in this study. The specimen with an exposure area of 1 cm^2 was utilized as the working electrode. Prior to the experiments, the samples were allowed to immerse in the test solution for 1h to promote a stable potential.

Cyclic voltammetry was performed at a scan rate of 50 mV/s, and the cyclic voltammograms were obtained over a voltage range of 1.5 to 0.5 V. Three cycles were recorded for each sample. The polarization curves were recorded potentiodynamically at 0.5 mV s^{-1}, and the potential scanning range was from lower than 200 mV of open-circuit potentials to the potential when the current indicated stable pitting occurrence.

The electrochemical impedance spectroscopy (EIS) measurement was conducted to analyze the electrochemical behavior of the passive film developed on the specimen surface. The frequency ranged from 0.01 Hz up to 100 KHz, with a 10 mV applied AC amplitude. The measured EIS data was fitted by the Zview 2.70 software. The passive films were formed by anodic polarization for 1 h at a -0.2 V potential. Following, the Mott-Schottky measurements were executed through a single frequency EIS at 1 kHz in the potential range of -1.0–1.0 V.

2.3 X-ray photoelectron spectrometer analysis

The chemical composition of the passive films was studied through the X-ray photoelectron spectroscopy. The curve was fitted by the commercial XPSPEAK software.

3. RESULTS AND DISCUSSION

3.1 The measurement of passive region

Figure 1 presents the cyclic voltammetric curves of three duplex stainless steels exposed to the simulated concrete pore solution. The two oxidation peaks and two reduction peaks were identified at three cycles. The oxidation peak at −1.1 V in Fig. 1 indicated the oxidation reaction of Fe:

$Fe+2OH \leftrightarrow Fe(OH)_2 + 2e$ (1)

In contrast, the oxide peak at -0.6V is relative to the formation of Fe_3O_4

$3Fe(OH)_2+2OH \leftrightarrow Fe_3O_4+ 4H_2O+2e$ (2)

When scanning was conducted continuously towards the positive potential, the high-sized passive region could be observed, signifying the transformation of Fe^{2+}/Fe^{3+}.

$Fe_3O_4+OH^-+ H_2O \leftrightarrow 3\gamma\text{-}FeOOH +2e^-$ (3)

$2Fe_3O_4+2OH^-+H_2O \leftrightarrow 3\gamma\text{-}Fe_2O_3+H_2O+2e^-$ (4)

The passive film was formed and gradually becoming thickened in the passive region. Consequently, the passive potential range of all 2101, 2205 and 2304 steels was approximately about -0.4~0.1 V.

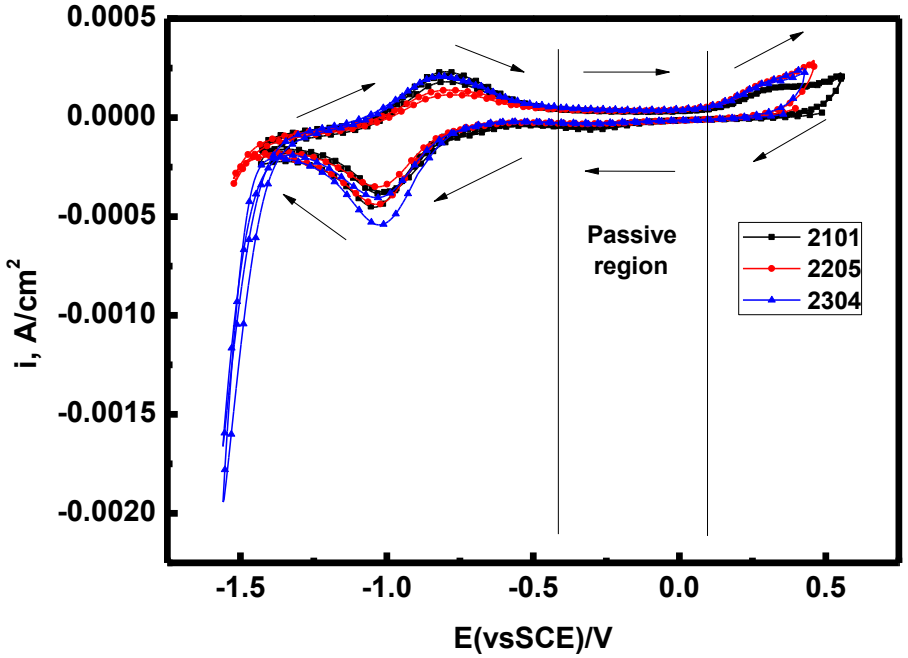

Figure 1. Cyclic voltammetric curves of three duplex stainless steels exposed to simulated concrete pore solution with PH 13.3

Potentiodynamic polarization measurement was executed on the samples with a fresh surface subsequently to 60 min of immersion. The typical polarization curves for three duplex steel in simulated concrete pore solution are presented in Fig. 2b. It could be observed that all samples for the three steels exhibited passive corrosion behavior, whereas the passive region was apparently observed in the samples, indicating the formation of compact passive film. The pitting potentials (E_{pit}) of the 2101, 2205 and 2304 DSS were approximately 0.5424V, 0.6024V and 0.5580V, respectively, which suggested that the pitting corrosion resistance followed the following sequence: 2205 >2304 > 2101. According to the regions of passivation ranges, the -0.2 V, 0 V and 0.1 V were selected to be utilized as the polarization potentials to prepare the passive film.

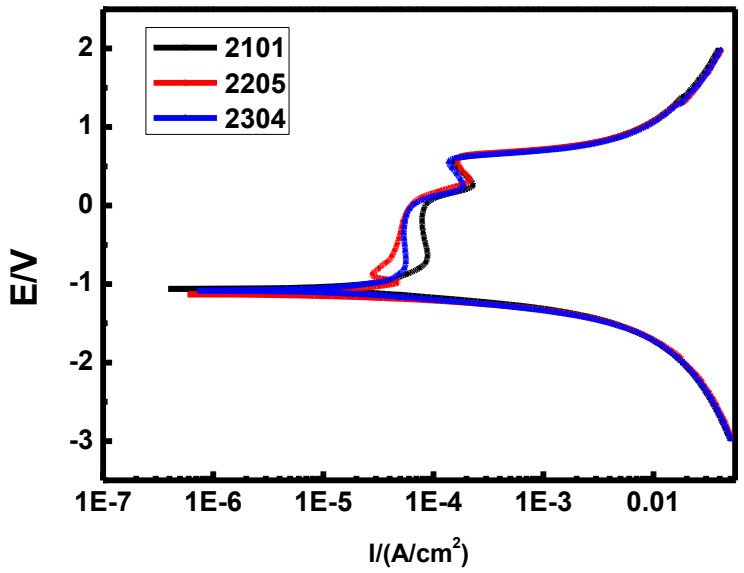

Figure 2. Dynamical polarization curves of three duplex stainless steels in simulated concrete pore solution with PH 13.3

3.2 Formation of passive film

In Figure 3, the real impedance was plotted vs. the imaginary impedance at each frequency for the duplex stainless steels passivated at different potential in the simulated concrete environment solution. It was observed that the Nyquist diagrams of the entire samples exhibited a depressed semicircle with a capacitive arc. In contrast, the diameter of the capacitive semicircle for the film formed at -0.2 V versus the SCE. was higher compared to the 0 and 0.1 V potentials. Furthermore, Figure 4 presents the plots of samples obtained at different potentials in the simulated concrete pore solution, where the phase angles and impedance amplitudes at -0.2 V versus SCE. were significantly higher compared to the samples passivated at 0 V and 0.1 V. Therefore, the formed passive films of the system at -0.2V were significantly stable compared to the other potentials.

Through the Bode plots of combinations Figures 3 and 4 with the characteristics of the passive film, the equivalent circuit in Figure 5 was proposed for the EIS data fitting to quantify the electrochemical parameters. In this equivalent circuit, the R_s was the solution resistance; Q_1 was the double charge layer capacitance; R_1 was the charge-transfer resistance. The electrochemical impedance parameters of the sample obtained from the EIS fitting diagrams are presented in Table 2. According to the fitting results, the changes to the solution resistance (R_s) were fairly minor for the samples, suggesting that the solution had no apparent change during the passive film formation. In contrast, the charge transfer resistance (R_1) of the 2101, 2205 and 2304 steels passivated at -0.2V were 4.926×10^5, 3.922×10^5 and 5.121×10^5 Ω cm^2, respectively, which were significantly higher than those formed at other passive potentials. Therefore, all duplex steel had the highest R1 at the -0.2V polarization potential, meaning that the passive films formed at -0.2V were the most compact.

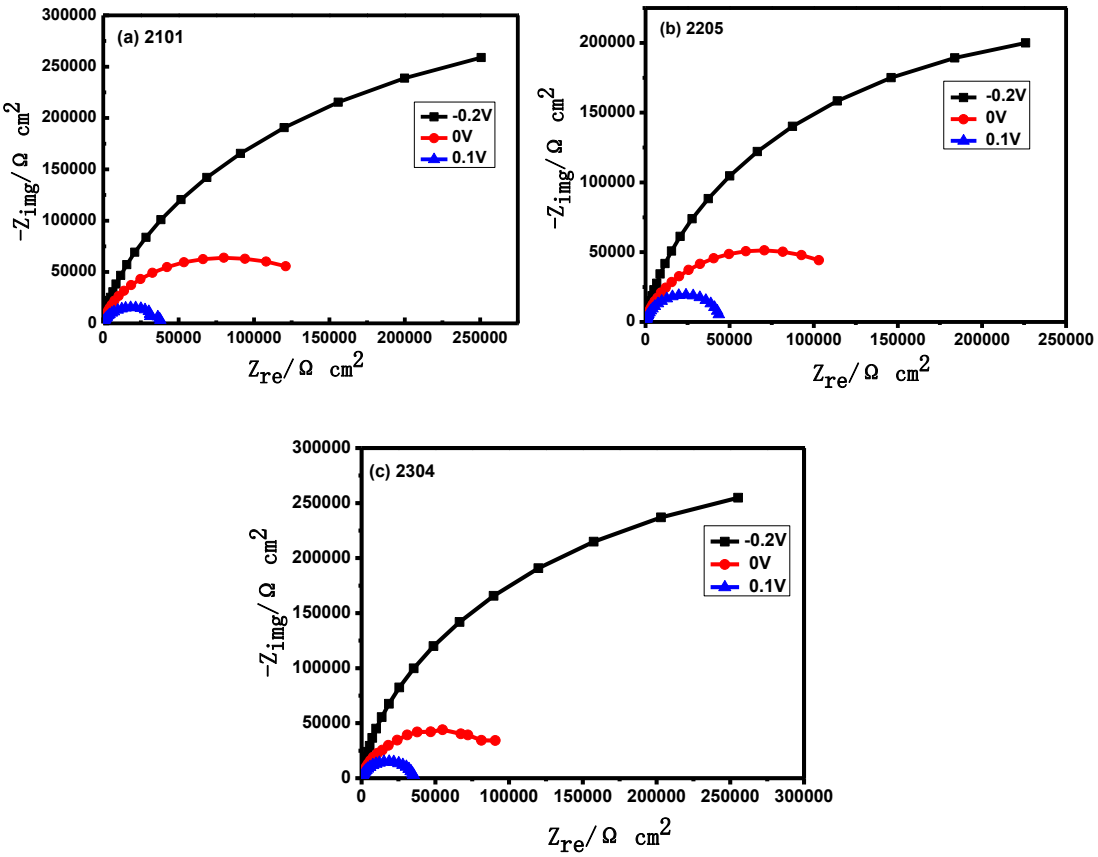

Figure 3. Nyquist plots of 2101, 2205 and 2304 DSS passivated at different potential in simulated concrete pore solution with PH 13.3

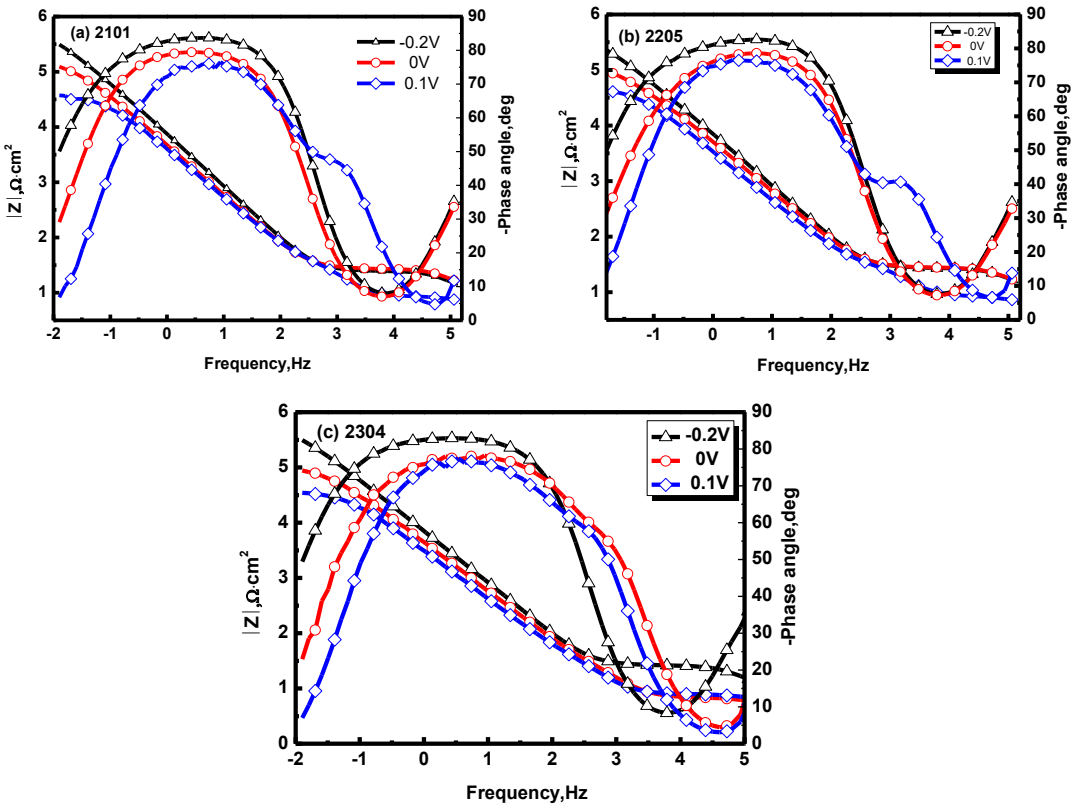

Figure 4. Bode curves of 2101, 2205 and 2304 DSS passivated at different potential in simulated concrete pore solution with PH 13.3

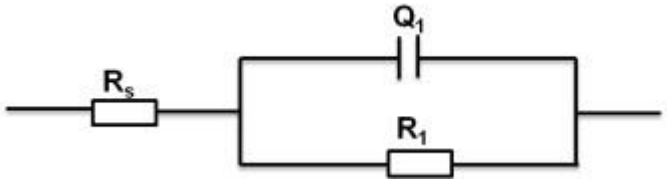

Figure 5. Equivalent circuits for impedance spectroscopy

Table 2. the fitting parameters of equivalent circuit components

Steel	Polarization voltage (V)	Rs $\Omega \cdot cm^2$	R_1 $\Omega \cdot cm^2$	Q_1	n
2101	-0.2	23.47	4.926×10^{5}	2.466×10^{-5}	0.9326
	0	8.499	4.162×10^{4}	5.480×10^{-5}	0.9185
	0.1	26.06	1.483×10^{5}	4.008×10^{-5}	0.9007
2205	-0.2	25.89	3.922×10^{5}	2.683×10^{-5}	0.9226
	0	26.23	1.193×10^{5}	3.976×10^{-5}	0.8843
	0.1	8.969	5.53×10^{4}	6.436×10^{-5}	0.9077
2304	-0.2	24.90	5.121×10^{5}	2.576×10^{-5}	0.9306
	0	6.859	1.091×10^{5}	4.565×10^{-5}	0.8625
	0.1	7.543	3.801×10^{4}	6.351×10^{-5}	0.8575

3.3 Capacitance results

To further investigate the formation of passive films on different duplex stainless steels, the Mott-Schottky plot as a powerful tool was utilized to record the carrier concentration of the passive film in the simulated concrete alkaline solution. Through the measurement of the capacitance of the Helmholtz layer and the space charge layer produced in the passive film, the semiconductor properties of the passive films could be investigated. Given the high generally large capacitance of the Helmholtz layer, it provided a slight contribution for the total capacitance; consequently, the measured capacitance of the film/electrolyte interface was approximately equal to the space charge capacitance. Therefore, the space charge capacitance of the p-type and n-type semiconductors can be calculated through the Equations (1) and (2), respectively [27].

Error! Reference source not found.Error! Reference source not found. (1) n-type

Error! Reference source not found. (2) p-type

where ε_0 is the vacuum permittivity (8.854×10^{-14} F/cm), ε is the relative dielectric constant, e is the electron charge (1.6×10^{-19}C), N_D and N_A are the donor and acceptor densities, respectively, E_f is the applied electrode potential, E_{fb} is the flat band potential, K is the Boltzmann constant (1.38×10^{-23} J/K); and T is the absolute temperature. Due to the measurements at room temperature, the kT/e could be neglected. The N_D or N_A could be obtained from the slope of the experimental C^{-2} versus E plots, based on Eq. (1) or Eq. (2).

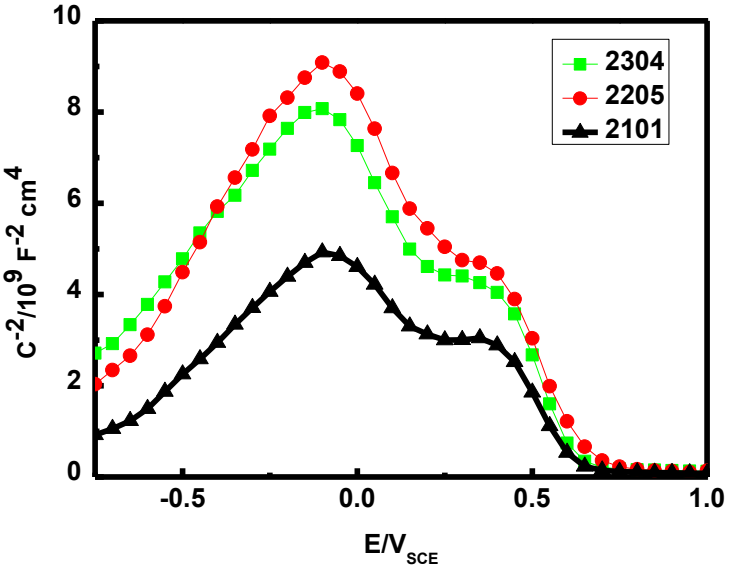

Figure 6. Mott-Schottky curve of passive film formed at -0.2 V polarization potential for 2101, 2205 and 2304 duplex stainless steel

Figure 6 presents the Mott-Schottky plots for the films formed on the duplex steels polarized in simulated concrete pore solutions for 1 h at -0.2V versus SCE. It could be observed that two apparent linear regions were presented in these plots which had a positive and negative slope representing different capacitances. The first region (R1) with positive slope, appearing for potentials bellow -0.20 V versus SCE., had the characteristics of n-type semiconductors. For potentials ranging from -0.20 to 0.20V versus SCE. (R2), the negative slopes stood for p-type semiconductors. A previous work on the passive film of stainless was utilized to confirm that there is dual layer structure on the passive film existed, which was composed by the chromium oxide inner layer and the iron oxide outer layer. For the chromium atom, the corresponding diffusion and reaction behavior at low potential can be described as follows:

$$Cr \rightarrow Cr^{3+} + 3e^- \quad (5)$$

$$2Cr^{3+} + 6OH^- \rightarrow Cr_2O_3 + 3H_2O \quad (6)$$

$$Cr^{3+} + 3H_2O \rightarrow Cr(OH)_3 + 3\ H^+ \quad (7)$$

For the iron atom, the corresponding anodic process at low potential is characterized as follows:

$$Fe \rightarrow Fe^{2+} + 2e^- \quad (8)$$

$$Fe^{2+} + 2OH^- \rightarrow Fe(OH)_2 \quad (9)$$

Therefore, the R_1 displayed the formation of n-type Fe_2O_3 and $Fe(OH)_3$ on the surface, whereas the R_2 represented the formation of the p-type Cr_2O_3 passive film. Figure 7 presents the calculated donor and acceptor densities for the films formed at various samples in simulated concrete solutions, respectively. It was apparent that the total acceptor concentration of N_A was always lower than the total donor concentration of N_D. Moreover, the doping concentration in the 2205 samples is higher compared to the 2101 and 2304 samples. The doping concentration was associated with the passive film, whereas the samples with increased doping concentration often had worse corrosion resistance.

Therefore, the 2205 exhibited the best corrosion resistance performance. The similar feature has been found in the 304, 316L, and 2205 DSS *et. al*. For example, Oguzie et al. reported that the presence of Cu in the passive film of 304, 430, 410 stainless steel increase the concentration of N_D and N_A values, thereby making the passive films not stability [28]. Lee et al. found that nitrogen alloying of 316L decreased the donor density and enrich the chromium on the passive film, causing the formation of a more stable passive film [29]. Lv suggested that the 2205 DSS treated by grain refinement promotes more Cr_2O_3 and Fe_2O_3 formed on the passive film, and decrease the doping concentration, which leads to a higher corrosion resistance than that of coarse grain in borate buffer solution [30].

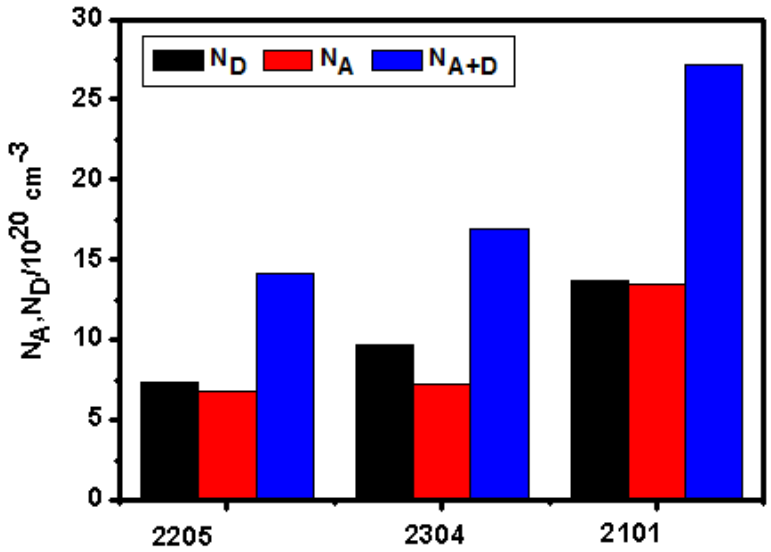

Figure 7. the acceptor concentration and donor concentration for different DSS samples

3.4 XPS characterization

The XPS spectra of three DSS subsequently to passivation at -0.2 V for 1 h in the simulated concrete solutions are presented in Figures 8-9, respectively. Both the metallic and oxidized states of the Cr 2p3/2 and the Fe 2p3/2 are presented. It was observed from the fitting results of the Cr 2p3/2 peaks that three constituent peaks existed, representing the metallic state Cr(met) (574.1 eV), the Cr_2O_3 (576.3 eV) and the $Cr(OH)_3$ (577.1 eV), respectively. In contrast, for the Fe 2p3/2 spectra presented in Figure 8, it could be separated into three or two constituent peaks, which represented the metallic state Fe (met) (707 eV) , the bivalent (Fe(II)) (709.4 eV) and the trivalent (Fe(III)) (711 eV) species. Moreover, the Fe(III) with a relative strong peak height indicated that the primary iron oxidized species were Fe(III) oxides in the passive film.

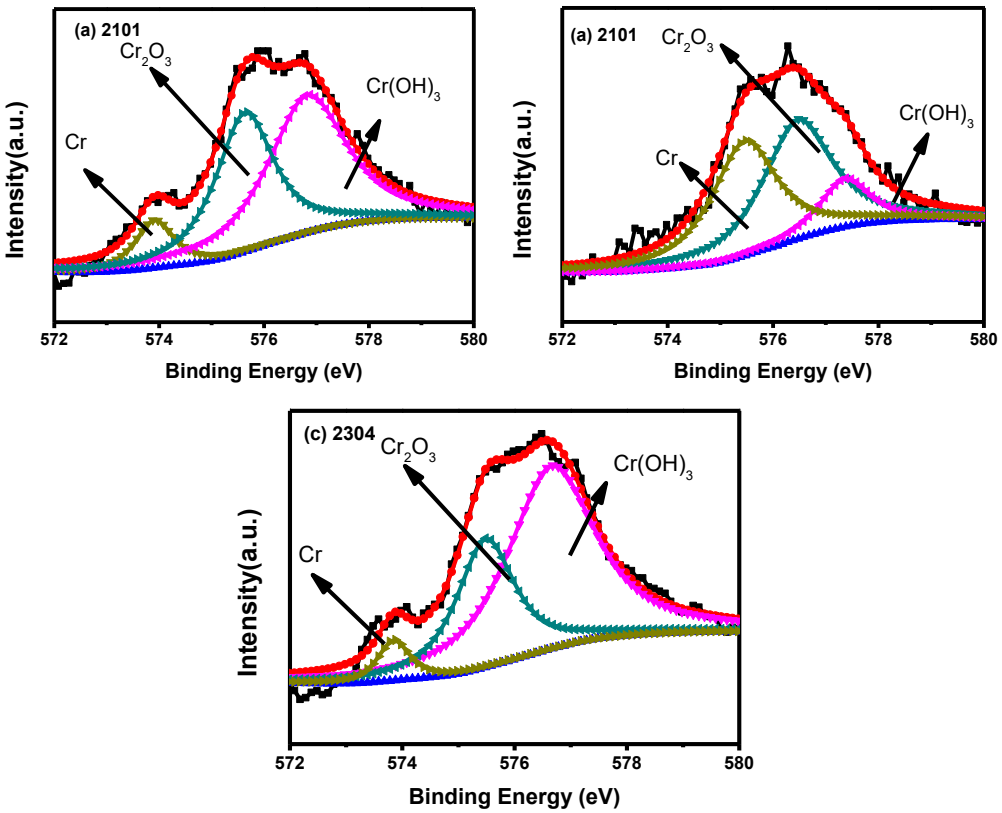

Figure 8. the detailed XPS spectra of Cr2p of the passive films formed on different DSS.

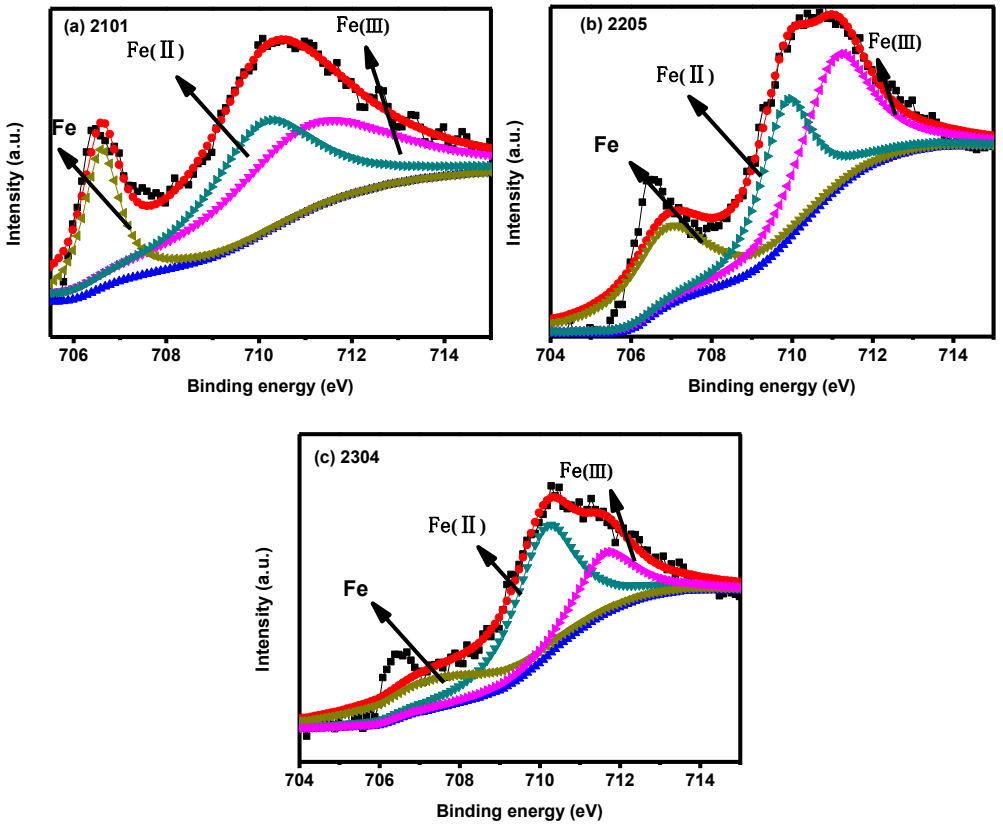

Figure 9. the detailed XPS spectra of Fe2p of the passive films formed on different DSS.

The presence of chromium in the passive film played a key role in the corrosion resistance of the stainless steel. The cationic fraction (C_x) was often utilized to characterize the composition of the passive film. Figure 10 presents the C_x values of Cr and Fe in the passive film, which were calculated through the following equation:

Error! Reference source not found. (10)

where C_x is the atomic percentage, Ix is the peak intensity corresponding to the area of the element M, and S_x is the sensitivity factor based on the XPS instrument. In this study, the sensitivity factors of Cr and Fe were 7.69 and 10.82, respectively [31]. The quantitative results suggested that the primary constituents of the passive film in the 2101 samples had relatively high contents of iron oxide species, whereas a higher quantity of chromium oxidized species existed in the passive film of the 2205 samples. In order to compare the chemical composition differences in passive film in higher details, the percentages of chromium and iron species were also researched. As presented in Figure 10, the 2101 samples had the enrichment of $Cr(OH)_3$ and the inhibition of Cr_2O_3, exhibiting a worse corrosion resistance compared to the other samples. Similar phenomena were also reported in the reported literature. The cationic fraction of Cr calculated by equation of 10 was relatively high in other stainless steels [32, 33], improving the stability of the passive film and the corrosion resistance. S.M. Alvarez et al. has studied the corrosion behavior of corrugated lean duplex stainless steels in different alkaline solutions, and they have found that 2304 shows better corrosion behavior than the 2101, but somewhat lower than the excellent behavior shown by 2205 [34]. Our result is similar to this study. In fact, it was proved that the corrosion resistance of the DSS would be enhanced as the Cr and Ni content increased. Consequently, the 2304 samples appeared to have the best corrosion resistance. In contrast, the higher Mo content in the 2205 and higher Mn content in the 2101 might have an effect on the corrosion resistance, which caused the formed passive film differences on the DSS surfaces in the simulated concrete environment.

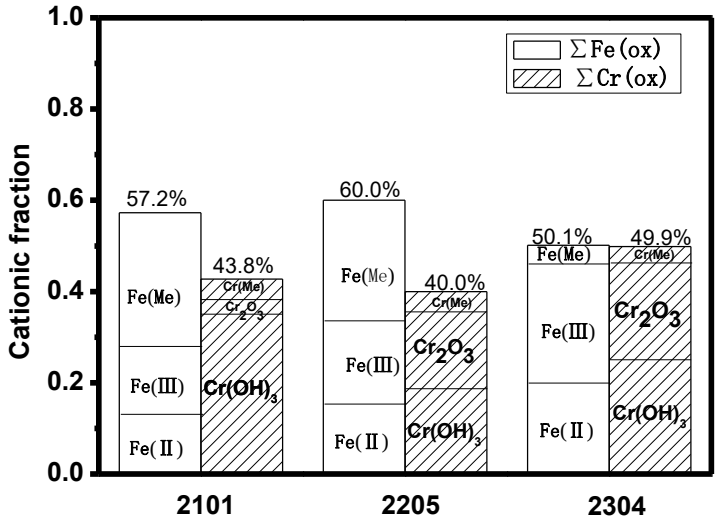

Figure 10. the XPS cationic fraction (C_x) in the passive film of different DSS

4. CONCLUSION

The passive ranges of the 2101, 2205 and 2304 duplex steels in simulated concrete pore solution with pH 13.0 were approximately -0.4-0.1V by means of cyclic voltammetry and potentiodynamic polarization curves. The electrochemical impedance spectroscopy confirmed the formation of passive films at -0.2 V as the most stable. The corrosion resistance of the 2101 samples was lower compared to the 2205 and 2304 samples, which occurred due to the significant increased donor and acceptor densities as well as inhibition of Cr_2O_3 on the passive film induced by the higher Mn content in the alloy composition. In contrast, the higher Mo content in the 2205 samples promoted the formation of Cr_2O_3 on the surfaces, leading to the best corrosion resistance.

ACKNOWLEDGEMENTS
This research was supported by the National Natural Science Foundation of China (Grant No. 51371123) and Shanxi Province Science Foundation for Youths (201601D202033).

References

1. A. Bautista, G. Blanco, F. Velasco, A. Gutiérrez, L. Soriano, F.J. Palomares, H. Takenouti, *Corros. Sci.* 51(2009) 785.
2. M.C. García-Alonso, M.L. Escudero, J.M. Mirando, M.I. Vega, F. Capilla, M.J. Correia, M. Salta, A. Bennani, J.A. González, *Cement Concrete Res.* 37(2007)1463.
3. P. Gu, S. Ellliot, J.J. Beaudoin, B. Arsenault, *Cement Concrete Res.* 26 (1996) 1151.
4. L. Veleva, A.A. Alpuche-Avilés, M.K. Graves-Brook, D.O. Wipf, *J. Electroanal. Chem.* 538 (2005) 45.
5. C.M. Abreu, M.J. Cristóbal, R. Losada, X.R. Nóvoa, G. Pena, M.C. Pérez, *Electrochim. Acta*, 49 (2004) 3049.
6. L. Freire, M.J. Carmezim, M.G.S. Ferreira, M.F. Montemor, *Electrochim. Acta*, 55 (2010) 6174.
7. J.O. Nilsson, *Mater. Sci. Tech.-Lond.*, 8 (1992) 685.
8. J. Gao, Y. Jiang, B. Deng, W. Zhang, C. Zhong, J. Li, *Electrochim. Acta* 54 (2009) 5830.
9. S. M. Alvarez, A. Bautista, F. Velasco, *Corros. Sci. 53* (2011) 1748.
10. H. Luo, C. F. Dong, X. G. Li, K. Xiao, *Electrochim. Acta*, , 64 (2012) 211.
11. R. D. Moser , P. M. Singh, L. F. Kahn, K. E. Kurtis, *Corros. Sci.* 57 (2012) 241.
12. T. J. Mesquita, E. Chauveau, M. Mantel, N. Kinsman, V. Roche, R. P. Nogueira, *Mater. Chem. Phy.*, 132 (2012) 967.
13. N. Ebrahimi, M. H. Moayed, A. Davoodi, *Corros. Sci.* 53 (2011) 1278.
14. M. Sumita, T. Hanawa, S. H. Teoh. *Mat. Sci. Eng. C-Mater.*, 24 (2004) 753.
15. A. Kocijan, Č. Donik, M. Jenko, *Corros. Sci.* 49 (2007) 2083.
16. E.M.A. Martini, I.L. Muller, *Corros. Sci.* 42 (2000) 443.
17. C. Boissy, B. Ter-Ovanessian, N. Mary, B. Normand, *Electrochim. Acta*, 174 (2015) 430.
18. E. Mccafferty, M.K. Bernett, J.S. Murday, *Corros. Sci.* 28 (1988) 559.
19. V. Schroeder, T.M. Devine, *J. Electrochem. Soc.* 146 (1999) 4061.
20. S. Mischler, H.J. Mathieu, D. Landolt, *Surf. Interface Anal.* 11 (1988) 182.
21. V. Vignal, O. Delrue, O. Heintz, J. Peultier, *Electrochim. Acta*, 55 (2010) 7118.
22. J. Lv, T. Liang, C. Wang, L. Dong, *J. Electroanal. Chem.* 757 (2015) 263.
23. S.P. Harrington, F. Wang, T.M. Devine, *Electrochim. Acta*, 55 (2010) 4092.
24. T. Li, L. Liu, B. Zhang, Y. Li, F. Wang, *Corros. Sci.* 104 (2016) 71.
25. Y. Wang, X. Cheng, X. Li, *Electrochem. Soc.* 57 (2015) 56.

26. J. Lv, H. Luo, *J. Mater. Eng. Per.* 23 (2014) 4223.
27. H. Luo, C.F. Dong, K. Xiao, X.G. Li, *Appl. Sur. Sci.* 258 (2011) 631.
28. E. E. Oguzie, J.B. Li, Y. Q. Liu, D. M. Chen, Y. Li, K. Yang, F. H. Wang, Electrochim. Acta, 55 (2010) 5028.
29. J. B. Lee, S. I. Yoon, Mater. Chem. Phy., 122 (2010) 194.34.
30. J. L. Lv, T. X. Liang, C. Wang, L. M. Dong, J. Electroanal. Chem., 757 (2015) 263.
31. C.T. Liu, J.K. Wu, *Corros. Sci.* 49 (2007) 2198.
32. H. Luo, H. Su, C. Dong, K. Xiao, X. Li, *Const. Build. Mater.*, 96 (2015) 502.
33. H. Luo, H. Su, C. Dong, X. Li, K. Xiao, *Electrochim. Acta*, 64 (2012) 211.
34. S.M. Alvarez, A. Bautista, F. Velasco, *Corros. Sci.* 53 (2011) 1748.